

# RSC Advances



This is an *Accepted Manuscript*, which has been through the Royal Society of Chemistry peer review process and has been accepted for publication.

*Accepted Manuscripts* are published online shortly after acceptance, before technical editing, formatting and proof reading. Using this free service, authors can make their results available to the community, in citable form, before we publish the edited article. This *Accepted Manuscript* will be replaced by the edited, formatted and paginated article as soon as this is available.

You can find more information about *Accepted Manuscripts* in the [Information for Authors](#).

Please note that technical editing may introduce minor changes to the text and/or graphics, which may alter content. The journal's standard [Terms & Conditions](#) and the [Ethical guidelines](#) still apply. In no event shall the Royal Society of Chemistry be held responsible for any errors or omissions in this *Accepted Manuscript* or any consequences arising from the use of any information it contains.



## Influence of CH<sub>4</sub>-Ar ratios on composition, microstructure and optical properties of Be<sub>2</sub>C films synthesized by DC reactive magnetron sputtering

Received 00th January 20xx,  
Accepted 00th January 20xx

DOI: 10.1039/x0xx00000x

www.rsc.org/

Yudan He,<sup>a</sup> Jiangshan Luo,<sup>a</sup> Kai Li,<sup>a</sup> Bingchi Luo,<sup>ab</sup> Jiqiang Zhang,<sup>a</sup> Hongbu Yin<sup>a</sup> and Weidong Wu<sup>ac\*</sup>

Beryllium carbide (Be<sub>2</sub>C) films were first deposited on optical quartz substrates by DC reactive magnetron sputtering of beryllium target with variable CH<sub>4</sub>-Ar ratios. The influence of CH<sub>4</sub>-Ar ratios on the compositions, microstructure and optical properties were investigated by X-ray photoelectron spectroscopy, X-ray diffraction, high resolution transmission electron microscope, atomic force microscopy, scanning electron microscope and UV-vis spectrum. The main component in films prepared at lower CH<sub>4</sub>-Ar ratios (< 5%) was Be<sub>2</sub>C and hydrocarbon (CH) films were formed at higher CH<sub>4</sub>-Ar ratios (> 15%). The films exhibited a nanocomposite structure consisting of Be<sub>2</sub>C nanocrystals (3 to 5 nm in size) embedded in amorphous hydrocarbon matrices. Smooth surface and columnar structure on the cross-section view were revealed. Besides, the depositing rates reached ~125 nm/h, which were significantly higher than that of rf reactive magnetron sputtering. High transparency (> 50%) of the Be<sub>2</sub>C films in the visible region as well as higher transparency (> 80%) in near infrared region were demonstrated. Finally, the dispersion of optical constants of Be<sub>2</sub>C films was presented and the optical bandgaps were evaluated to be ~2 eV. The good properties of Be<sub>2</sub>C films prepared by dc reactive sputtering showed that this material could be a potential candidate for application to inertial confinement fusion targets.

### 1. Introduction

Recently, many concerns have been paid to the low Z (atomic number) materials due to their important usages in nuclear fusion researches.<sup>1-3</sup> Beryllium carbide (Be<sub>2</sub>C), as a typical low Z material, was reported to be a promising wall material choice for the next generation experimental fusion reactor ITER because it mitigated not only the pure beryllium but also the pure carbon sputtering yields.<sup>4,5</sup> Another important application was for inertial confinement fusion (ICF) capsule materials. The most principle requirements for capsule materials are low atomic number, smooth surface, uniform composition and structures, and high density.<sup>6-8</sup> Doped beryllium and hydrocarbon (CH) coatings were the most commonly selected target materials in National Ignition Facility (NIF).<sup>6-11</sup> Currently, the compound (Be<sub>2</sub>C) caught researchers' attentions because it combined the advantages of beryllium and hydrocarbon.<sup>12,13</sup> Comparing with hydrocarbon, Be<sub>2</sub>C owns lower atomic number (Z=4.7), higher density (ρ=2.4 g/cm<sup>3</sup>) and mechanical strength (bulk modulus B<sub>0</sub>=217.05 GPa and shear modulus C<sub>s</sub> = 165.95 GPa).<sup>2,3,14</sup>

Comparing with beryllium, its antifluorite structure results in the smoother surface and grain refinement, and it is yellowish-brown transparent crystals with bandgap over 1.2~2 eV,<sup>3,14</sup> which might indicate that the deuterium-tritium (D-T) ice layers in Be<sub>2</sub>C capsules could be characterized by optical methods and homogenized by infrared heating.<sup>15</sup> Comprehensive understandings of its optical properties were needed to evaluate this advantage.

Due to its important usages, the structural, electronic and optical properties of beryllium carbide have been adequately investigated by theoretical calculations.<sup>1-3,16</sup> On the experimental side, however, only few literatures could be referred. Beryllium carbide was firstly synthesized by Lebeau and its structural properties were studied.<sup>14,17</sup> Thereafter, Xie and Shih etc. deposited beryllium carbide coatings by plasma polymerization of diethyl-beryllium and rf reactive magnetron sputtering for application to ICF.<sup>13,18,19</sup> The H<sub>2</sub> permeability, mechanical properties, chemical composition, electrical and thermal conductivities of beryllium carbide films were analysed. The results indicated that most of the requirements of the ignition target were satisfied. However, some shortcomings existing in these two methods limited their applications to ICF targets. First, the instability and long recovery time of saturation vapor pressure of diethyl-beryllium<sup>20</sup> made it hard to control the composition, let alone its high cost. Moreover, doping was difficult to come true in deposition by plasma polymerization. Second, the maximum deposition rate was ~56 nm/h by rf reactive magnetron sputtering<sup>21</sup>, which was too low for depositing targets. To the best of our knowledge, the optical properties of beryllium carbide has

<sup>a</sup> Research Center of Laser Fusion, China Academy of Engineering Physics, Mianyang, 621900, China.

<sup>b</sup> Science and Technology on Plasma Physics Laboratory, Mianyang 621900, China.

<sup>c</sup> IFSA Collaborative Innovation Center, Shanghai Jiao Tong University, Shanghai 200240, China.

\*. E-mail: [wuwaidongding@163.com](mailto:wuweidongding@163.com); Tel: +86 0816 2480903.

not to date been researched experimentally, while, it is important for application to ICF targets. The scarcity of experimental optical studies is due to the nature of the Be<sub>2</sub>C samples: Be<sub>2</sub>C is a high toxicity component, which is difficult to prepare and tends to hydrolyse and oxidize.<sup>3</sup>

In present works, Be<sub>2</sub>C films were firstly prepared by dc magnetron sputtering beryllium into methane plasma. The compositions were controlled by the CH<sub>4</sub>-Ar ratio during sputtering process. Carbon content in films increased with the increase of CH<sub>4</sub>-Ar ratio and hydrocarbon films were formed at CH<sub>4</sub>-Ar ratio >15%. Based on this finding, the Be<sub>2</sub>C films were in situ covered by a layer of hydrocarbon (~26 nm), which was demonstrated to be effective in preventing oxidation. In addition, the microstructures and morphologies were determined. Finally, the optical properties of Be<sub>2</sub>C films were measured by a double-beam spectrophotometer for the first time, and it gave an optical bandgap about 2 eV.

## 2. Experimental

### 2.1. Preparation of Be<sub>2</sub>C films

Beryllium carbide films were deposited on optical quartz substrates by dc reactive magnetron sputtering of a 76-mm-diameter beryllium target under various CH<sub>4</sub>-Ar ratios at room temperature. The flow rates of argon and methane were accurately controlled by mass flow controllers, where the flow rate of Ar was fixed at 50 sccm while the flow rate of CH<sub>4</sub> varied (0.8, 1.0, 1.2, 1.5, 2.0, 2.5, 3.0, 5.0, 7.5 and 10 sccm correspond to CH<sub>4</sub>-Ar ratios of 1.6%, 2.0%, 2.4%, 3.0%, 4.0%, 5.0%, 6.0%, 10%, 15% and 20%, respectively). An angle ~45° existed between the plane of target and substrate. The distance between the Be target and substrates was set to be ~90 mm. In order to reduce the possibility of target poisoning, argon was introduced near the target and methane was introduced near the substrates. The system was evacuated to a base pressure of  $1.0 \times 10^{-5}$  Pa. Before the deposition, the substrate shutter was closed and pre-sputtering was conducted on the Be target to remove any contaminants and to guarantee a fresh beryllium surface. During the growth, the working pressure was maintained at 0.5 Pa and the sputtering power was constant at 50 W. The substrate was rotated at constant rate of 6 rpm to improve the uniformity. The depositing time was controlled to be 4 hours. After the deposition, protective layers (~26 nm hydrocarbon) were in situ covered on the surface of the Be<sub>2</sub>C films, which were prepared at 1.6-5.0% CH<sub>4</sub>-Ar ratio, by simply increasing the CH<sub>4</sub> flow rate up to 10 sccm and sustaining 8 minutes. A 26 nm hydrocarbon film was deposited on quartz substrate as a reference sample for morphology and optical property measurements.

### 2.2. Characterization of Be<sub>2</sub>C films

The elemental composition and their corresponding chemical states of different Be<sub>2</sub>C films were studied by the X-ray (Mg-K $\alpha$  1253.6 eV) photoelectron spectroscopy (XPS). The microstructure was investigated by X-ray diffraction (XRD) with grazing angle mode using Cu K $\alpha$  ( $\lambda = 0.154056$  nm) radiation, as well as high resolution transmission electron microscope

(HRTEM). For HRTEM measurement, the film (deposited at 2.4% CH<sub>4</sub>-Ar ratio) was scratched with a sharp razor blade in the ethanol environment. Then, it was dispersed in ethanol and fished on the TEM grid. The surface and cross-section morphologies were observed by atomic force microscopy (AFM) and scanning electron microscope (SEM), respectively. The root mean square (RMS) surface roughness of the films was evaluated over a  $1 \times 1 \mu\text{m}^2$  area. The deposition rates were calculated from the thickness (measured by SEM) and deposition time. The average densities were evaluated from the weight gain and thickness of films with definite area. The optical properties were analysed from the transmittance and reflectance spectrum measured by a double-beam spectrophotometer, which has two beams of light, one for measurement and the other for reference. When testing, the Be<sub>2</sub>C films were placed on the testing sample holder and the freshly deposited ~26 nm hydrocarbon on quartz substrate (reference sample) was placed on the reference sample holder. Thus, the obtained spectrum only showed the response of the Be<sub>2</sub>C films.

## 3. Results and discussion

### 3.1. Composition analysis

Fig. 1(a) shows partial XPS survey spectra of films deposited under different CH<sub>4</sub>-Ar ratios from 1.6% to 20% after 30 mins Ar<sup>+</sup> etching to remove any surface contaminants and protective layers. It confirmed the chemical purity of the films, as it only consisted of Be, C, and O, and no peaks corresponding to other elements were detected. The binding energy of O<sub>1s</sub> peak was about 533.1 eV in all samples, which suggested that its chemical state remained unchanged. Nevertheless, appreciable shifts were observed in C<sub>1s</sub> and Be<sub>1s</sub> peaks, indicating changes in chemical states of carbon and beryllium. In order to identify the chemical states and relative amount of each element in that state, high resolution XPS spectra of Be, C and O were conducted, in which overlapped band were deconvoluted into separate peaks by Gaussian fitting using XPS peakfit software. Partial typical high resolution XPS spectra of beryllium and carbon were illustrated in Fig. 1(b) and Fig. 1(c), respectively. The peaks centred at 111.23, 112.42, 114.55 eV in Be<sub>1s</sub> high resolution spectra were assigned to metallic Be, Be<sub>2</sub>C, and BeO, respectively.<sup>22</sup> And peaks at 282.46, 284.54, 286.23, 288.17 eV in C<sub>1s</sub> high resolution spectra were attributed to Be<sub>2</sub>C, CH, C-O and C=O species, respectively.<sup>21,22</sup> It was found that the presence of hydrocarbon increased with the increasing of CH<sub>4</sub>-Ar ratios. When the CH<sub>4</sub>-Ar ratios were below 5%, the major chemical state (> 50 mol%) of beryllium and carbon peaks were beryllium carbide. Beryllium was not incorporated in the depositions and hydrocarbon films were formed when the CH<sub>4</sub>-Ar ratios were beyond 15% (shown in Fig. 1(c)). Besides, a small amount of metallic beryllium existed in films prepared at lower CH<sub>4</sub>-Ar ratios (2.0% and 1.6%).

The atomic concentrations of elements and their relative amount in each chemical state were calculated from the peak areas with corresponding sensitivity factors, as plotted in Fig. 2. It was found that the beryllium content decreased while the carbon content increased gradually with the increasing of CH<sub>4</sub>-

Ar ratios in the range of 1.6%-5% (Fig. 2(a)), leading to the reduction of Be-C ratios from 2.11 to 1.26 (Fig. 2(b)). Further increasing the CH<sub>4</sub>-Ar ratio resulted in a dramatic decreasing of the beryllium content and increasing of the carbon content, until pure hydrocarbon films were formed. The results were non-consistent with previous research<sup>20</sup>, where the Be-C ratios reached 3.5 when the CH<sub>4</sub>-Ar ratio was 25% and maintained at ~1 even when the CH<sub>4</sub>-Ar ratio exceeded 50%. However, the variation trend of the beryllium and carbon content with the CH<sub>4</sub>-Ar ratios in our work was the same as theirs. Taking account of the difference in the experiment configuration and parameters, the distinction was understandable. The higher sputtering power (200W) used in their experiments was more effective for beryllium sputtering, resulting in the higher Be-C ratio. The percentage of beryllium (Be\*) and carbon (C\*) bonded as Be<sub>2</sub>C as a function of CH<sub>4</sub>-Ar ratios in the range of 1.6%

to 5% were illustrated in Fig. 2(b). The major (> 85%) chemical state of beryllium was in Be<sub>2</sub>C, meanwhile, the percentage of carbon bonded as Be<sub>2</sub>C decreased with the increasing of CH<sub>4</sub>-Ar ratios. However, the atomic ratios of Be\* and C\* always remained close to 2, which fitted the stoichiometric of Be<sub>2</sub>C, suggesting the accuracy of the XPS analysis.

The XPS analysis also suggested that oxidation had been effectively controlled by protective coverages since only little oxygen existed in films with CH<sub>4</sub>-Ar ratios < 5%, comparing with the fact that the uncovered Be<sub>2</sub>C films were quickly oxidized and delaminated after exposing to ambience (not shown). This was also confirmed by films deposited at 6% and 10% (uncovered), where all beryllium was in its oxidation state and the oxygen content reached 34.3 at% and 32.2 at%, respectively.

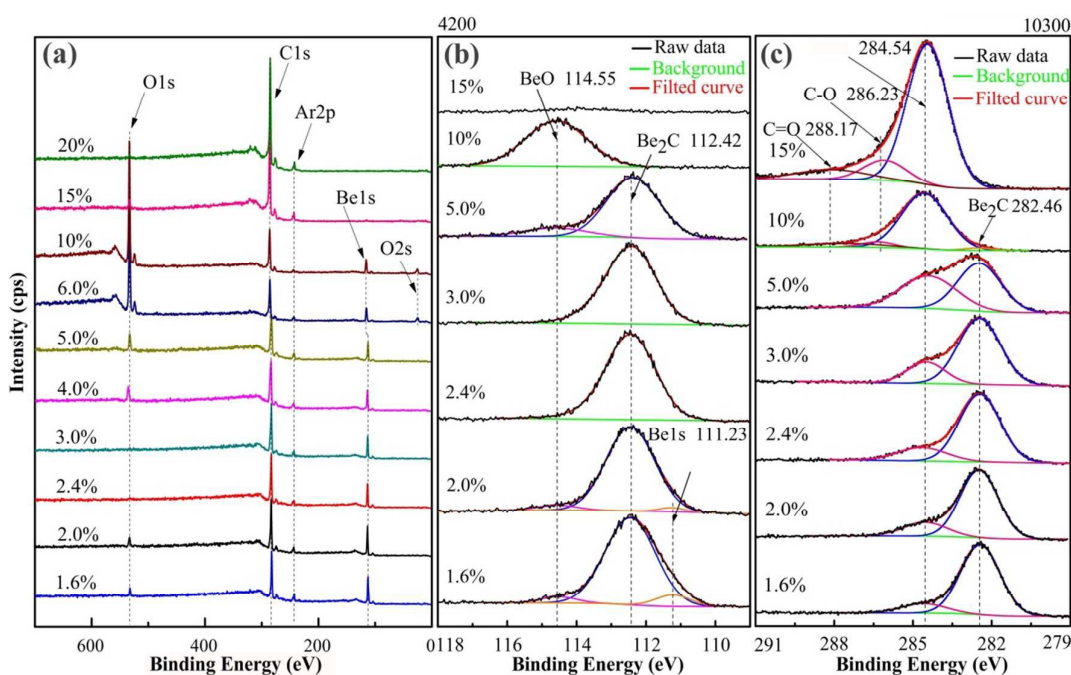


Fig.1 XPS spectra for films prepared at different CH<sub>4</sub>-Ar ratios after 30mins Ar<sup>+</sup> etching survey spectrum (a), deconvolution of Be<sub>1s</sub> peaks (b) and deconvolution of C<sub>1s</sub> peaks (c).

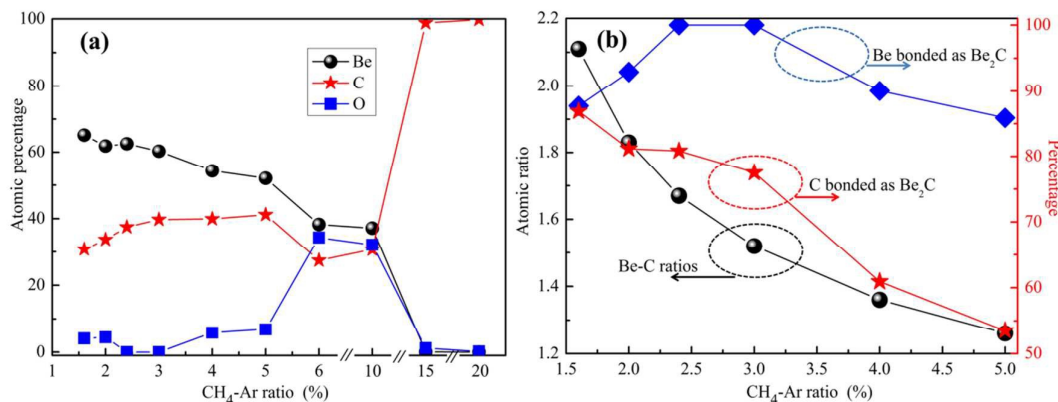


Fig.2 (a) The atomic content of Be, C and O in films with various CH<sub>4</sub>-Ar ratios. (b) The atomic ratios of Be-C, as well as the percentage of Be and C bonded as Be<sub>2</sub>C for films deposited at different CH<sub>4</sub>-Ar ratios.

XRD measurements were also performed on films for structural investigations. Fig. S1 (supplementary data) shows the XRD patterns of as-deposited  $\text{Be}_2\text{C}$  films with various  $\text{CH}_4$ -Ar ratios. There were no obvious diffraction peaks in the XRD patterns. Further measurements should be introduced to reveal the microstructure. In Ref.<sup>23,24</sup>, the microstructure of Be-related materials ( $\text{Be}_{1-x}\text{B}_x$  and  $\text{BeN}$ ) were measured by TEM.

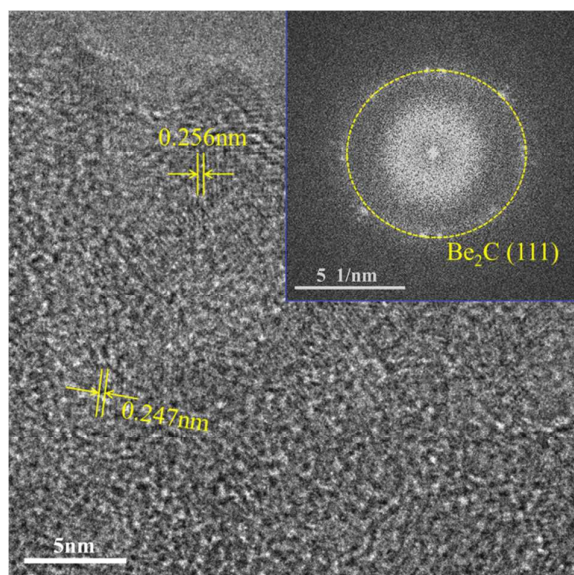


Fig.3 Plane view high-resolution TEM image and corresponding FFT pattern (inserted in upper-right) for film obtained at 2.4%  $\text{CH}_4$ -Ar ratio.

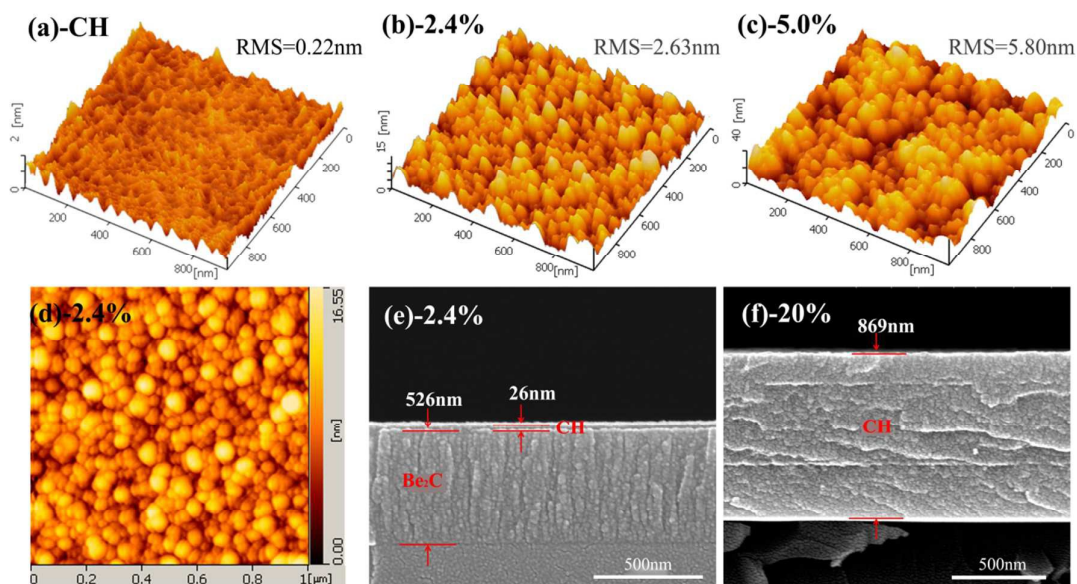


Fig. 4 Typical surface morphologies (AFM 3-dimension images) of (a)  $\sim 26$  nm hydrocarbon film on the quartz substrate as a reference sample,  $\text{Be}_2\text{C}$  films deposited at (b) 2.4%, (c) 5.0%  $\text{CH}_4$ -Ar ratio and (d) AFM 2-dimension image for  $\text{Be}_2\text{C}$  films deposited at 2.4%  $\text{CH}_4$ -Ar ratio. Cross-section morphologies (SEM images) for films deposited at (e) 2.4% and (f) 20%  $\text{CH}_4$ -Ar ratio.

HRTEM observation was performed on films deposited at 2.4%. Fig.3 represents the plane view HRTEM image and its corresponding Fast Fourier transform (FFT) pattern (inserted in upper-right). The HRTEM image demonstrated the nanocomposite structure of the films, where  $\text{Be}_2\text{C}$  nanocrystals (3-5 nm) distributed in amorphous matrixes. The interplanar spacing was found to be  $0.251 \pm 0.005$  nm, referring to the (111) plane of  $\text{Be}_2\text{C}$  phase (PDF-33-0191)<sup>25</sup>. The FFT pattern exhibited the clear diffraction ring attributed to the (111) plane of  $\text{Be}_2\text{C}$ . Although there was  $\sim 19\%$  hydrocarbon in the film (determined by XPS analysis), no diffraction rings corresponding to carbon was detected, which might indicate that the amorphous matrixes consisted of hydrocarbons. This nanocomposite structure was widely found in films prepared by reactive sputtering at room temperature with low sputtering power.<sup>26</sup> In these conditions, atoms ejected from the target surface with low kinetic energy could not get extra energy from the substrates to reach competent diffusion rate when they were adsorbed on the surface of substrates, resulting in the formation of nanocomposite structure. The influence of the sputtering power and substrate temperature on the depositions was also investigated and would be discussed in other works.

Generally, nanocrystalline phase is detectable in the XRD spectrum.<sup>27</sup> However, there were no obvious peaks in the XRD patterns of those nanocomposite  $\text{Be}_2\text{C}$  films. This might attribute to two aspect reasons: a) The low atomic number of  $\text{Be}_2\text{C}$  resulted in difficulty in XRD detection;<sup>28</sup> b) The films in this work were too thin and the grain size was too small for  $\text{Be}_2\text{C}$  to produce obvious X-ray diffraction peaks.

### 3.2. Film morphologies and growth characteristics

The surface and cross-section morphologies films under various CH<sub>4</sub>-Ar ratios were studied using AFM and SEM, respectively. Partial typical surface and cross-section morphologies are displayed in Fig. 4. The AFM images of Be<sub>2</sub>C films at 2.4% CH<sub>4</sub>-Ar ratio clearly showed that many small spherical shaped granules (20~70 nm in diameter and 0~20 nm in height) homogeneously distributed over the surfaces. As the increasing of CH<sub>4</sub>-Ar ratio, small particles tended to merge into larger ones, resulting in the greater RMS roughness at higher CH<sub>4</sub>-Ar ratios. The surface morphologies and RMS roughness of the ~26 nm hydrocarbon films (reference sample) were also examined. It presented a non-characteristic surface with very low surface roughness ~ 0.22 nm (shown in Fig. 4(a)). Thus, it was convinced that the granular morphologies and roughness were mainly attributed to Be<sub>2</sub>C films instead of hydrocarbon protective layers. The measured RMS roughness of films deposited at 1.6%, 2.0%, 2.4%, 3.0%, 4.0% and 5.0% were 2.51, 2.19, 2.63, 2.82, 3.31 and 5.80 nm, respectively. It suggested that the surface roughness of the Be<sub>2</sub>C films increased with the increasing of CH contents. Since the smooth surface is significant for its application in ICF targets, the purer Be<sub>2</sub>C films are desirable. The typical surface morphologies (3-dimension views) for the ~26 nm thick hydrocarbon film (reference sample), films prepared at 2.4% and 5.0% were illustrated in Fig. 4(a), (b) and (c), respectively. Surface morphologies for Be<sub>2</sub>C films at 1.6%, 2.0%, 3.0% and 4.0% CH<sub>4</sub>-Ar ratio were shown in supplementary data Fig. S2. Typical 2-dimension view morphology (deposition at 2.4%) was also given in Fig. 4(d). Columnar structures always existed when the CH<sub>4</sub>-Ar ratio was below 5%, as revealed by the cross-section views. As a contrast, homogeneous morphology without columnar and other characteristic structure was revealed in hydrocarbon films. Here, we only presented the typical cross-section morphologies for samples prepared under 2.4% and 20%, as illustrated in Fig. 4(e) and Fig. 4(f), respectively. The lamination in Fig. 4(f) was resulted from the fractionated deposition owing to the target poisoning under high CH<sub>4</sub>-Ar ratios.

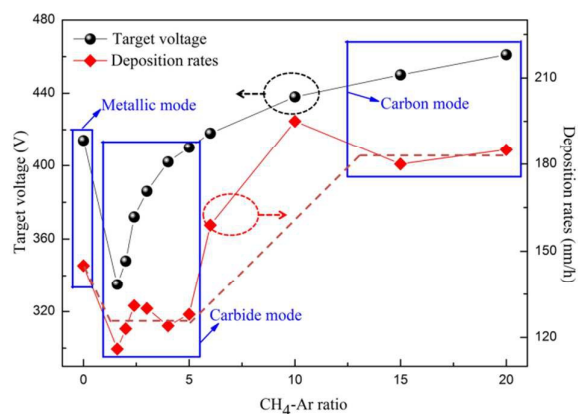


Fig. 5 Deposition rates and target voltages versus CH<sub>4</sub>-Ar ratios.

The coating thickness was evaluated from the cross-section views and the deposition rates were calculated from the thickness with defined deposition time. The variation of deposition rates with CH<sub>4</sub>-Ar ratios might imply changes in sputtering modes which could be also monitored by target voltages. Fig. 5 exhibited the deposition rates and target voltages as a function of CH<sub>4</sub>-Ar ratios. The introduction of a handful of methane (1.6%) resulted in remarkable deterioration of the deposition rates. The deposition rates were relative stable (~125nm/h) over the range of 1.6% to 5.0% and increased to be ~182nm/h in the range of 15%-20%. The deposition rates in our work (dc reactive magnetron sputtering) were much higher that reported in Ref.<sup>21</sup> (rf reactive magnetron sputtering) and it could be further improved by increasing sputtering power (not shown in this work). The higher deposition rate was beneficial to depositing ICF capsules. Oxidation in films deposited at 6% and 10% led to an increasing thickness, resulting in the abnormal high deposition rates. Combining with XPS analysis, we suspected that there were three sputtering modes during the depositions as the CH<sub>4</sub>-Ar ratio varied from 0-20%: (a) metallic sputtering mode in which the depositions mainly consisted of metallic beryllium, (b) compound sputtering mode where a thin layer of carbide was formed on the target surface and the depositions mainly consisted of beryllium carbide, (c) non-metallic sputtering mode in which hydrocarbon coated on the target surface and the depositions were hydrocarbon. The formation of hydrocarbon made it more complicated than other reactive sputtering (oxide and nitride). The variations of target voltages followed the similar trend with that of deposition rates. Target voltages in metallic mode was higher than that in compound mode and lower than that in non-metallic mode, as shown in Fig. 5. The results owned good repeatability. Therefore, we suspected that the target voltage can be used as a symbol for judging the status of sputtering.

Based on the thickness and weight gain of films with defined area (15×15mm<sup>2</sup>), the average density was calculated. The average densities decreased from 1.94 to 1.68 g/cm<sup>3</sup> with the increasing of CH<sub>4</sub>-Ar ratios from 1.6% to 5.0%, which were smaller than Be<sub>2</sub>C films prepared by PECVD<sup>13</sup> but bigger than that of hydrocarbon films<sup>9</sup>. The comparative low density might be caused by the incorporation of hydrocarbons. And it could be improved by optimizing experiment parameters such as sputtering power and annealing temperature (not studied in this work).

### 3.3. Optical properties

The deposited Be<sub>2</sub>C films varied from deep reddish-brown (1.6%) to light orange (5.0%). In order to evaluate the optical properties of Be<sub>2</sub>C films, the optical transmittance and reflectance spectra were measured over the wavelength range of 200-2000 nm. Fig. 6 shows the optical transmittance spectrum of Be<sub>2</sub>C films deposited with various CH<sub>4</sub>-Ar ratios (1.6-5.0%). Apparent interference feature could be observed in every spectrum, which was universal in transparent films and implied the smooth and homogeneous surface. The optical transmittance

increased with the increasing of CH<sub>4</sub>-Ar ratios. For Be<sub>2</sub>C films without metallic beryllium, the average transmittance was greater than 55% in visible region (500 to 760 nm) and beyond 80% in near infrared region. This suggested that it was feasible to characterize the deuterium-tritium (D-T) ice layers by optical methods and to homogenize by infrared heating in Be<sub>2</sub>C capsules.

The dispersion of absorption coefficient was calculated using transmittance and reflectance data combining with the thickness. The transmittance and reflectance spectra were fitted by envelope methods before being adopted to eliminate the influence of interference and one typical fitting curve was inset in Fig. 6. The absorption coefficient is computed by:<sup>29</sup>

$$\alpha(\lambda) = \frac{1}{d} \ln \left( \frac{1-R(\lambda)}{T(\lambda)} \right) \dots (1)$$

where  $d$  is the thickness measured by SEM,  $R(\lambda)$  is the reflectance and  $T(\lambda)$  is the transmittance.

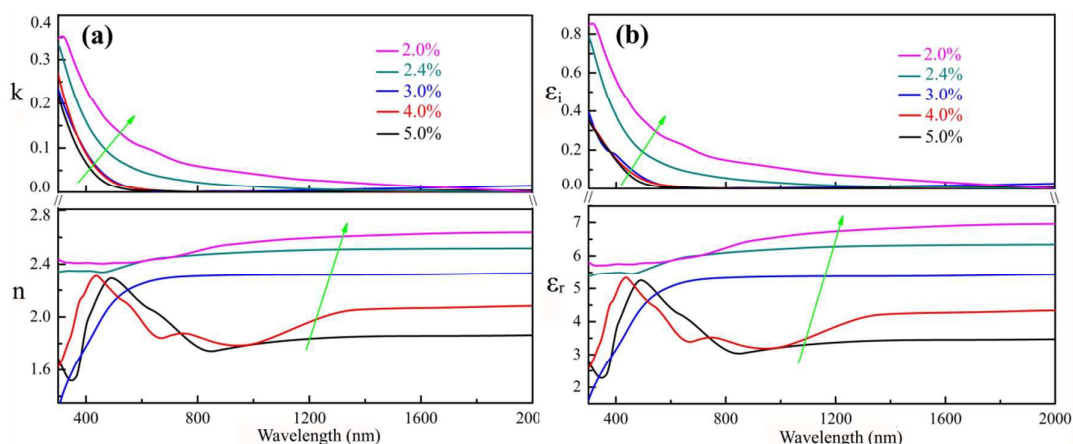


Fig. 7 (a) Dispersion curves of extinction coefficient ( $k$ ), refractive index ( $n$ ) and (b) the variation of real ( $\epsilon_r$ ), imaginary ( $\epsilon_i$ ) parts of the dielectric constant with wavelength for Be<sub>2</sub>C films deposited at 2.0-5.0% CH<sub>4</sub>-Ar ratios.

The dispersion behaviour of optical constants, as we all know, plays an important role in the research for optical materials and can be readily achieved from the following equations:<sup>29, 30</sup>

$$k(\lambda) = \frac{\lambda \alpha(\lambda)}{4\pi} \dots (2)$$

$$n(\lambda) = \frac{1+R(\lambda)}{1-R(\lambda)} + \sqrt{\left(\frac{1+R(\lambda)}{1-R(\lambda)}\right)^2 - (1+k^2(\lambda))} \dots (3)$$

$$\epsilon_r(\lambda) = n^2(\lambda) - k^2(\lambda) \dots (4)$$

$$\epsilon_i(\lambda) = 2n(\lambda)k(\lambda) \dots (5)$$

where  $\alpha(\lambda)$  is the absorption coefficient calculated from equation (1),  $k(\lambda)$  is the extinction coefficient,  $n(\lambda)$  is the refractive index,  $\epsilon_r(\lambda)$  is real parts and  $\epsilon_i(\lambda)$  is the imaginary parts of the complex dielectric constant. The dispersion curves of extinction coefficient ( $k$ ), refractive index ( $n$ ), variation of real ( $\epsilon_r$ ) and imaginary ( $\epsilon_i$ ) parts of the dielectric constant are illustrated in Fig. 7. As can be seen, the extinction coefficient ( $k$ ) and refractive index ( $n$ ) tended to increase when the CH<sub>4</sub>-Ar ratios decreased. The variations in refractive index could be attributed to the difference in densities. According to the Lorentz-Lorenz

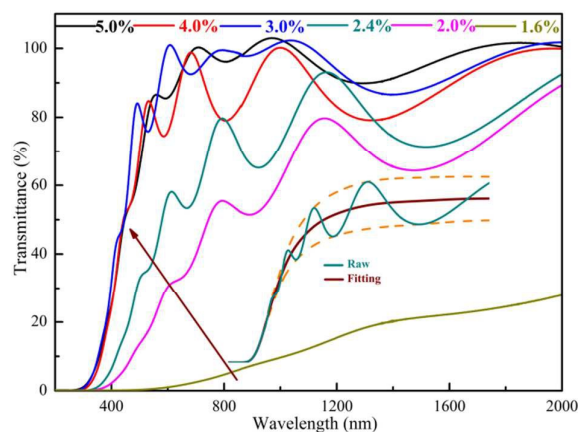


Fig. 6 Optical transmittance spectra of the Be<sub>2</sub>C films prepared with different CH<sub>4</sub>-Ar ratios.

formula<sup>31</sup>  $\alpha(\lambda) = \frac{3}{4\pi N} \frac{n^2(\lambda)-1}{n^2(\lambda)+2}$  (where  $\alpha(\lambda)$  is the mean polarizability,  $N$  is the number density of molecules), the refractive index ( $n$ ) increases with the increasing of densities. In addition, for the purer Be<sub>2</sub>C films (deposited at 2.4%) the refractive index ( $n$ ) and real parts of dielectric constant ( $\epsilon_r$ ) in infrared region are 2.52 and 6.34, respectively, which are extraordinary close to theoretical calculation values (2.50 for  $n$ , and 6.25 for  $\epsilon_r$ ).<sup>2</sup>

The optical bandgaps were determined from the absorption coefficient via the Tauc relation<sup>26</sup> by extrapolating the linear region of the  $(\alpha h\nu)^{1/2}$ - $h\nu$  plot to energy axis, where the exponent 1/2 is for indirect bandgap. Fig. 8 shows the Tauc analysis, which gives optical bandgaps of 2.43, 2.21, 2.10, 2.03, 1.7 and 0.37 eV for films deposited with CH<sub>4</sub>-Ar ratios of 5.0%, 4.0%, 3.0%, 2.4%, 2.0% and 1.6%, respectively. Theoretical calculations on Be<sub>2</sub>C using the GGA and LDA functional revealed an indirect bandgap about 1.2eV located between  $\Gamma$  and X.<sup>1,2,16</sup> However, the electron energy loss spectra (EELS) data determined an experimental correction to the gap of  $\sim$ 2eV.<sup>3</sup> This value was close to the obtained optical bandgaps. Decreasing in

the optical bandgaps with the decreasing of CH<sub>4</sub>-Ar ratio was founded, which might be related to the compositions. The larger optical bandgaps for films with CH<sub>4</sub>-Ar ratios of 5.0% and 4.0% might result from the presence of beryllia (bandgap ~10.6eV<sup>32</sup>). The Be<sub>2</sub>C film deposited at 1.6% owns the smallest bandgap (0.37eV), which is probably due to the existence of metallic beryllium in the films as revealed by XPS analysis. The comparison with the other experiment literature has proven to be difficult as the optical properties of beryllium carbide films have been barely investigated.

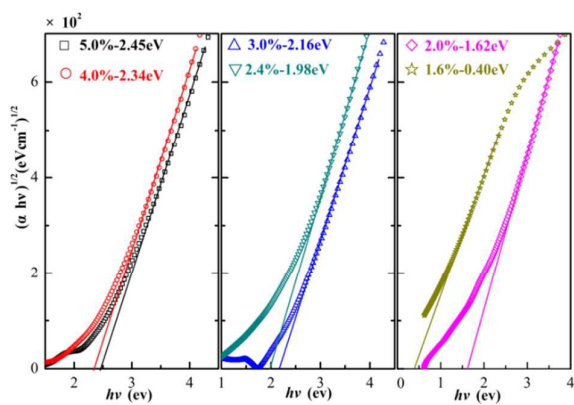


Fig. 8 Plots of  $(\alpha hv)^{1/2}$  versus photon energy  $h\nu$  and extrapolating for optical bandgaps ( $E_g$ ) for Be<sub>2</sub>C films under various CH<sub>4</sub>-Ar ratios.

#### 4. Conclusions

In summary, Be<sub>2</sub>C films were firstly prepared by dc reactive magnetron sputtering on optical quartz substrates with various CH<sub>4</sub>-Ar ratios and characterized by suitable analytical techniques. The XPS results revealed that the hydrocarbon content in films increased with the increasing of CH<sub>4</sub>-Ar ratios, meanwhile, beryllium carbide was the main component (> 50 mol%) in films prepared with lower CH<sub>4</sub>-Ar ratios (< 5%) and hydrocarbon films were obtained when the CH<sub>4</sub>-Ar ratios exceed 15%. Based on this finding, protective coatings (~26nm CH) were in situ deposited on Be<sub>2</sub>C films, which was proved to be effective in preventing oxidation. HRTEM images clearly showed that nanocrystal Be<sub>2</sub>C particles were embedded in amorphous hydrocarbon matrices. The films exhibited smooth surface and columnar structure on the cross-section view as presented by AFM and SEM. In our experiments, the deposition rates (~125 nm/h) were higher than that of rf sputtering, which was favourable for depositing inertial confinement fusion (ICF) capsules. The optical measurements unfolded the high transparency of Be<sub>2</sub>C films from visible light to near infrared (500-2000 nm), suggesting the feasibility of characterizing the deuterium-tritium (D-T) ice layers by optical methods and homogenizing by infrared heating in Be<sub>2</sub>C capsules. In addition, the dispersion of optical constant was investigated. The obtained optical bandgap ( $E_g$ ), refractive index ( $n$ ) and real part of dielectric constant ( $\epsilon_r$ ) for the purer Be<sub>2</sub>C films (deposited at CH<sub>4</sub>-Ar ratio of 2.4%) are 1.98 eV, 2.52 and 6.34, respectively,

and are in accordance with the theoretical calculations. The results showed that this material could be a potential candidate for application to ICF capsules.

#### Acknowledgements

This work was financially supported by the National Key Science Foundation of China (Grant NO. 2014YQ090709). The authors would like to acknowledge Yong Zeng and Dr. Qi Yang for their help in testing. The authors also are grateful to Xiulan Tan and Dr. Zhengwei Xiong for their beneficial discussions.

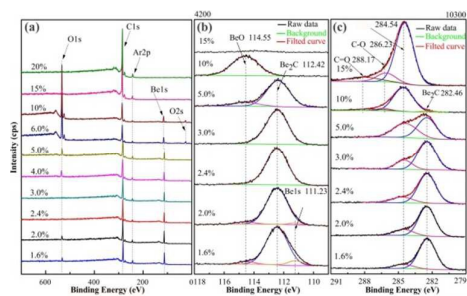
#### References

- 1 C. H. Lee, W.R. L. Lambrecht and B. Segall, *Phys. Rev. B*, 1995, **51**(16), 10392-10398.
- 2 S. Laref and A. Laref, *Comput. Mater. Sci.*, 2008, **44**(2), 664-669.
- 3 C. -T. Tzeng, K. -D. Tsuei, and W. -S. Lo, *Phys. Rev. B*, 1998, **58**(11), 6837-6843.
- 4 M. Mehine, C. Björkas, K. Vörtler, K. Nordlund and M. I. Airilaet, *J. Nucl. Mater.*, 2011, **414**(1), 1-7.
- 5 R. Mateus, P. A. Carvalho, N. Franco, L. C. Alves, M. Fonseca, C. Porosnicu and E. Alves, *J. Nucl. Mater.*, 2013, **442**(1), S320-S324.
- 6 A. N. Simakov, D. C. Wilson, A. Y. Sunghwan, J. L. Kline, D. S. Clark and S. H. Batha, *Phys. Plasma*, 2014, **21**(2), 022701.
- 7 JET Team, *J. Nucl. Mater.*, 1990, **176**, 3-13.
- 8 A. J. MacKinnon, N. B. Meezan, J. S. Ross, S. L. Pape, L. B. Hopkins and et al., *Phys. Plasma*, 2014, **21**, 056318.
- 9 S. W. Haan, J. D. Salmonson, D. S. Clark, D. D. Ho, B. A. Hammel, D. A. Callahan and et al., *Fusion Sci. Technol.*, 2011, **59**(1), 1-7.
- 10 B. C. Luo, K. Li, X. L. Tan, J. Q. Zhang, J. S. Luo, W. D. Wu and Y. J. Tang, *J. Alloys Compd.*, 2014, **607**, 150-156.
- 11 B. A. Hammel and the National Ignition Campaign Team, *Plasma Phys. Controlled Fusion*, 2006, **48**(12B), B497-B506.
- 12 R. Brusasco, S. Letts, P. Miller, M. Saculla and R. Cook, *Vac. Sci. Technol. A*, 1996, **14**(3), 1019-1024.
- 13 W. S. Shih, R. B. Stephens and W. J. James, *Fusion Sci. Technol.*, 2000, **37**(1), 24-31.
- 14 M. W. Mallett, E. A. Durbin, M. C. Udy, D. A. Vaughan and E. J. Center, *J. Electrochem. Soc.*, 1954, **101**(6), 298-305.
- 15 B. C. Luo, K. Li, Y. D. He, G. Niu, J. Q. Zhang, J. S. Luo, W. D. Wu and Y. J. Tang, *High Power Laser and Particle Beams*, 2013, **25**(12), 2359-2365.
- 16 F. Kalarasse, B. Bennecer, *J. Phys. Chem. Solids*, 2008, **69**(7), 1775-1781.
- 17 J. H. Coobs, W. J. Koshuba, *J. Electrochem. Soc.*, 1952, **99**(3), 115-120.
- 18 Y. X. Xie, R. B. Stephens, N. C. Morosoff and W. J. James, *J. Fusion Energy*, 1998, **17**(3), 259-260.
- 19 W. S. Shih, N. E. Barr, W. J. James, N. C. Morosoff and R. B. Stephens, *Fusion Sci. Technol.*, 1997, **31**(4), 442-448.

## Paper

## RSC Advances

- 20 R. Brusasco, S. Letts, P. Miller, M. Saculla, R. Cook, *J. Vac. Sci. Technol. A*, 1996, **14**(3), 1019-1024.
- 21 Y. X. Xie, Plasma deposition of beryllium carbide via magnetron sputtering [D], Rolla: Univ. of Missouri, 1998.
- 22 Y. X. Xie, N. C. Morosoff and W. J. James, *J. Nucl. Mater.*, 2001, **289**, 48-51.
- 23 A. F. Jankowski, M. A. Wall and T. G. Nieh, *J. Non-cryst. Solids*, 2003, **317**(1), 129-136.
- 24 A. F. Jankowski, M. A. Wall, A. W. Van Buuren, T. G. Nieh and J. Wadsworth, *Acta Mater*, 2002, **50**, 4791-4800
- 25 Powder Diffraction File (PCPDFWIN v.2.02), 1999 JCPDS-International Centre for Diffraction Data, 33-0191.
- 26 J. Nazon, J. Sarradin, V. Flaud, J. C. Tedenac and N. Frety, *J. Alloys Compd.*, 2008, **464**(1), 526-531.
- 27 S. Mehraj, M. S. Ansari and Alimuddin, *Thin Solid Films*, 2015, **589**, 57-65.
- 28 Y. D. He, J. S. Luo, J. Li, L. B. Meng, B. C. Luo, J. Q. Zhang, Y. Zeng and W.D. Wu, *Fusion Eng. Des.*, 2016, **103**, 118-124.
- 29 Y. Xin, H. Zhou, X. Ni, Y. Pan, X. Zhang, J. Zheng, S. Bao and P. Jin, *RSC Adv.*, 2015, **5**(71), 57757-57763.
- 30 J. M. Khoshman, A. Khan and M. E. Kordesch, *Appl. Phys.*, 2007, **101**, 103532.
- 31 K. E. Oughstun and N. A. Cartwright, *Opt. Express*, 2003, **11**(13), 1541-1546.
- 32 A. L. Ivanovskii, I. R. Shein, Y. N. Makurin, V. S. Kiiko and M. A. Gorbunova, *Inorg. Mater.*, 2009, **45**(3), 223-234.



The XPS results revealed that the hydrocarbon content in films increased with the increasing of CH<sub>4</sub>-Ar ratios, meanwhile, beryllium carbide was the main component in films prepared with lower CH<sub>4</sub>-Ar ratios (< 5%) and hydrocarbon films were obtained when the CH<sub>4</sub>-Ar ratios exceed 15%.